Advances in Clinical Radiology 1 (2019) 1–17
ADVANCES IN CLINICAL RADIOLOGY

State-of-the-Art Dual-Energy Computed Tomography in Gastrointestinal and Genitourinary Imaging

Ashish Khandelwal, MD[a], Achille Mileto, MD[b], Shuai Leng, PhD[a], Joel G. Fletcher, MD[a,*]
[a]Mayo Clinic, 200 First Street Southwest, Rochester, MN 55905, USA; [b]University of Washington, 325 9th Avenue, Seattle, WA 98104, USA

KEYWORDS
• Dual energy • Computed tomography • CT • Gastrointestinal • Liver • Kidney • Small bowel
• Genitourinary

KEY POINTS
- Dual energy computed tomography can be performed at similar radiation doses to single energy scans and offers increased diagnostic benefit in abdominopelvic imaging.
- Routine reconstructions for most tasks include virtual monoenergetic images, virtual noncontrast images, and iodine maps, supplemented by the ability to perform iodine or fat quantification.
- The ability of dual energy to discriminate iodine enhancement from other causes of increased computed tomography attenuation has diagnostic benefit for diagnosis involving the kidneys, pancreas, and bowel.
- Iodine and fat quantification are being used increasingly in dual energy computed tomography practice as problem solving tools.
- Although a wide variety of existing and emerging computed tomography systems perform dual energy imaging, standardization of practice is making interpretation routine.

INTRODUCTION

Dual-energy computed tomography (DECT) scanning was first introduced commercially in 2006 with the production of a dual-source CT system, with each x-ray tube using different tube energies [1,2]. Other commercial implementations including a single tube system with rapid kV switching and single tube dual layer x-ray detector systems were subsequently introduced [3,4], with additional multispectral technologies continuing to emerge [5]. The basic principle of DECT scanning is to generate an image from the datasets obtained by using attenuation differences at different energy levels from the same anatomic region. DECT scanning has the ability to increase iodine signal and materially classify tissues according to composition, and the clinical workflow and displays offered by different manufacturers initially differed substantially. Over the past 12 years, however, there has been increasing evidence showing the diagnostic benefit of DECT scanning and increasing standardization of this technology in CT clinical practice [6–8]. The purpose of this review is to highlight patient benefits and advances in DECT scanning that have led to integration into abdominal CT clinical practice.

Conflict of Interest Disclosure: No conflicts for any author.

*Corresponding author, *E-mail address:* fletcher.joel@mayo.edu

https://doi.org/10.1016/j.yacr.2019.04.011
2589-8744/19/

CONSIDERATIONS WHEN DESIGNING ACQUISITION AND RECONSTRUCTION PROTOCOLS

For designing acquisition and reconstruction protocols for DECT scanning, standard single energy protocols of the same anatomic region and indication can be used as references. Special considerations and changes can be made according to the clinical need and the DE techniques available using the specific scanners.

In general, most DECT protocols are designed using the same or similar radiation dose as that of standard single energy CT scanning, that is, dose-neutral DECT protocols. However, in certain scenarios where DECT scanning provides critical information for diagnosis that is not available in single energy CT scans, the clinical benefits justify a higher radiation dose. Radiation dose matching is achieved by adjusting scanning techniques, especially tube current (mA) or mAs, to match the volume CT dose index between single and DECT protocols. Most DE systems offer an option to reconstruct single energy-like images (eg, mixed kV images) that use all of the photons used for image creation and have comparable image quality as the standard single energy CT images at the same dose level. In addition, virtual monoenergetic images (VMI) at lower keV have similar or higher contrast-to-noise ratios than single energy images, using an energy domain noise reduction technique [9,10].

Patient size should be carefully considered in DECT examinations. For all DECT systems, the low-energy beam may be problematic for large patients owing to its low penetration power (high attenuation); image artifacts and excessive noise in these patients could affect multienergy analysis and clinical diagnosis. The specific size limit depends on the specific scanner model and the DECT technology. For systems with multiple DECT modes available, scanning techniques should be adapted to patient size (eg, for a dual source system, 80/Sn150 kV is used to achieve the best energy separation for small patients, whereas 100/Sn150 kV should be used for large patients owing to the better penetration capability of the 100 kV). For all DE systems, a size limit should be set at which no obvious artifacts or excessive noise observed, and patients larger than this size limit should undergo single energy CT scanning.

In addition to the scanning techniques, image reconstruction should also be considered carefully in DECT protocols, because this factor will particularly influence quantitative parameters. In single energy CT scans, reconstruction kernels with edge enhancement are commonly used to improve visualization of boundaries of anatomy and pathology. These kernels, however, may not be appropriate for DECT applications because the edge enhancement may change CT numbers, which consequently affects material decomposition and other DECT applications. Quantitative kernels that maintain CT number accuracy are usually used in DECT reconstructions. Slice thickness should also be considered carefully in DECT scans. In addition to the conventional balance between noise and resolution in single energy CT scans, material decomposition in DECT scans tends to enhance image noise. Therefore, too thin slices may result in excessive noise in postprocessed images, whereas slices that are too thick may increase partial volume effect and consequently affect CT number. Similar to single energy CT scans, iterative reconstruction algorithms are now commonly used in DECT applications to reduce image noise or radiation dose. For dual source DECT scans, reconstruction field of view of DE is limited to the scanning field of view of the second detector (26–35 cm). It should be carefully aligned to ensure all anatomy and pathology of interest is fully encompassed inside the DE field of view.

ORGAN-SPECIFIC ADVANCES AND USES

Genitourinary System

Adrenal nodule evaluation

Adrenal nodules are commonly discovered serendipitously on routine contrast-enhanced CT examinations obtained for a variety of clinical complaints [11,12]. Although it has been shown that the majority of incidentaloma adrenal lesions are indolent adenomatous lesions [11,12], incomplete characterization leads to additional imaging tests to rule out an adrenal malignancy (eg, adrenal metastases, carcinoma, or lymphoma) [11,12].

DECT scans with synthesis of virtual unenhanced datasets from contrast-enhanced data provides a viable option to characterize adrenal incidentalomas when conventional unenhanced images are unavailable [13,14]. Virtual noncontrast (VNC) images render a good approximation of conventional unenhanced images (Fig. 1) [13,14], but yield a slight degree of discrepancy (ie, 5–10 Hounsfield units) in comparison with conventional noncontrast images, thus limiting the adoption of the widely accepted +10 Hounsfield unit threshold method for DECT scans [13,14].

More recently, DECT software allow for quantifying the presence of fat using material decomposition algorithms [15,16]. DECT fat fraction estimates

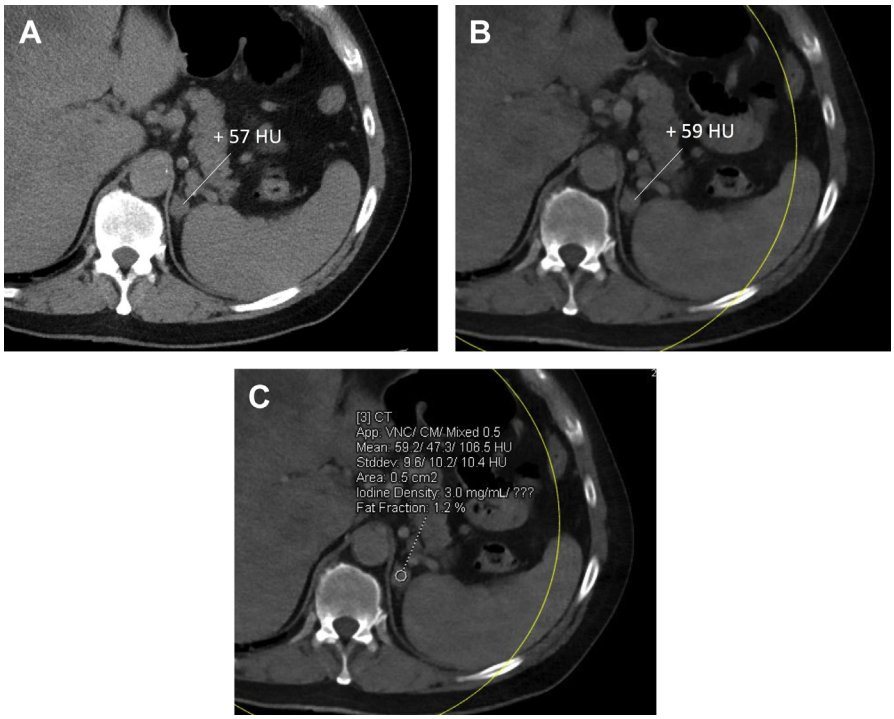

FIG. 1 Conventional (**A**) noncontrast and (**B**) VNC images in a 56-year-old man with metastatic renal cell carcinoma with left adrenal metastasis. Note the substantial agreement in CT number between the 2 series. (**C**) Fat fraction calculated from DECT data show negligible amount of intralesion fat, confirming the nonadenomatous nature of the lesion.

intralesional fat using a 3-material decomposition algorithm on the dual-source DECT systems [15–17]. Single-source DECT systems with fast kV switching use a slightly different approach with synthesis of binary image datasets (eg, fat–iodine images) where fat can be indirectly quantified in relative quantities (in milligrams per milliliter) [15–17]. These techniques have shown encouraging initial findings [15–17]. Alternatively, VMI can be used to identify nonadenomatous lesions by demonstrating substantially higher attenuation levels at high keV settings (ie, 140 keV) [18].

Renal stone characterization

Determination in vivo of renal stone types has paramount clinical value because it can aid the clinical management of patient [19]: urine alkalization is the mainstay of treatment for uric acid–based stones, whereas percutaneous treatments can be necessary for non-uric acid–based stones [19,20].

DECT scanning characterizes renal stones by exploiting material attenuation knowledge at high and low energy levels [19] and depends on the degree of spectral separation and DECT number ratio (ie, attenuation of a given material on the low-energy image to the attenuation on the high-energy image) [20]. Based on the DECT number ratio, a given stone is assigned an arbitrary color coding with one of the commercially available system displaying non-uric acid–based, calcium-containing stones in blue color, whereas uric acid-based stones are color coded in red (Fig. 2).

DECT scanning has a diagnostic accuracy approaching 100% for differentiating non-uric acid–based calcium-containing stones from uric acid stones in small to medium size phantoms and patients [19,21]. The recent advent of tin filtration along with the ability to select different DECT tube energies (eg, 90/150 Sn kV or 100/150 Sn kV) have enhanced the discrimination power of DECT scanning across a wider range of patient body sizes [21,22], and emerging photon-counting CT systems promise to increase spatial resolution and spectral separation to further improve detection and noninvasive characterization of renal stones [23].

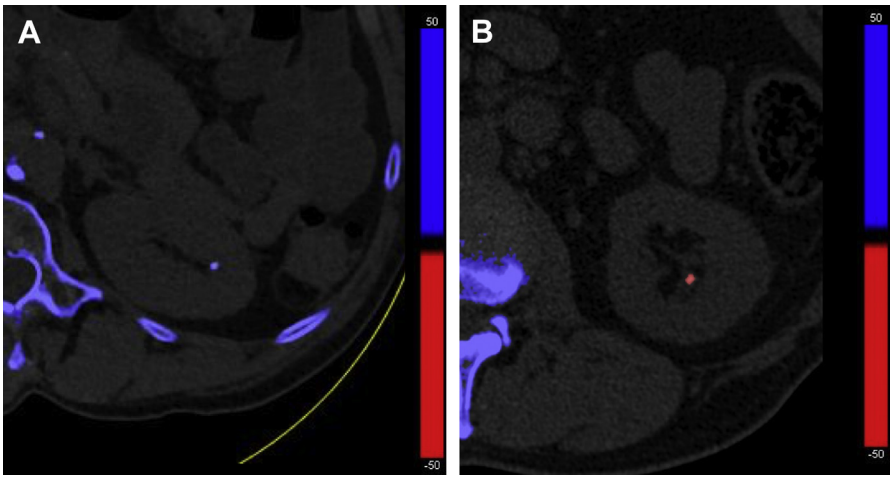

FIG. 2 DECT color-coded image in 2 patients with nonobstructing calyceal tip stones. (**A**) Image shows color-coded stone in blue indicating non–uric acid content (ie, calcium-containing). (**B**) Image of another patient shows a color-coded stone in red indicating uric acid content.

Renal mass evaluation

The number of incidentally discovered renal masses is continuously increasing given the use of cross-sectional imaging [24], and a single contrast-enhanced series cannot distinguish a nonenhancing hemorrhagic cyst from a solid enhancing neoplasm [24,25].

DECT scans can improve the image-based evaluation of serendipitously encountered renal masses [26]. Material decomposition algorithms enable the selective identification of iodine, which can be either subtracted from contrast-enhanced data to create a VNC image or selectively displayed in a color-coded fashion to generate an iodine map (Fig. 3) [26–30].

VNC images are a good qualitative and quantitative approximation for evaluating precontrast features of renal masses (eg, the presence of fat or calcifications) [28] and may result in a decrease in the radiation dose if used to replace noncontrast series [26,28]. Iodine maps are probably the most useful series for renal mass characterization by discriminating between nonenhancing renal cysts and enhancing neoplasms showing varying degrees of iodine uptake [31–33] (see Fig. 3). Iodine maps also provide more quantitative information by enabling direct estimation of region of interest-based iodine, which is useful for differentiating low levels of enhancement (eg, type 1 papillary renal cell carcinoma) from high-attenuation nonenhancing cysts [31]. It is important to recognize that different threshold values for iodine enhancement should be used for different vendors [34]. For example, the diagnostic threshold of 0.5 mg/mL for dual source DECT scanning reflects the traditional 20-Hounsfield units change in attenuation between precontrast and postcontrast scans [31].

Fat quantification and atomic number mapping from contrast-enhanced data may further the application spectrum of DECT scans in renal mass evaluation [35].Using material decomposition, intralesional fat can be detected and estimated either by using absolute percentage (ie, fat fraction) or relative milligrams per milliliter values [36], which may be helpful to detect fat-containing renal masses (Fig. 4).

GASTROINTESTINAL SYSTEM

Liver Mass Evaluation

Contrast-enhanced, multiphase CT scans for the evaluation or detection and characterization of liver lesions or neoplasms is one of the most common diagnostic tasks in abdominal CT scans. Detection of hepatocellular carcinoma (HCC) in at-risk patients with chronic liver disease is a model for how DECT scans can benefit multiphase liver CT scans. For HCC, imaging criteria are used for diagnosis, and the detection of small enhancing lesions and tumor washout are critical for determining transplant eligibility [37].

The ability of DECT scans to potentiate iodine signal and iodine signal differences is therefore useful diagnostically in these patients, and can be performed without increasing radiation dose [38]. Arterially

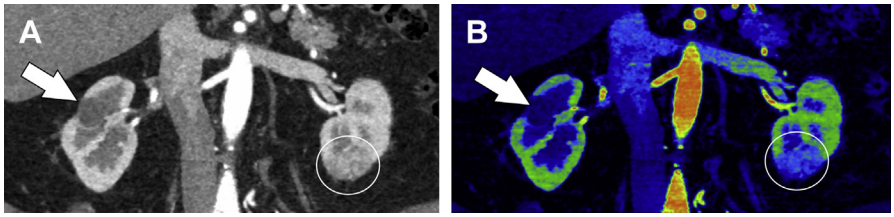

FIG. 3 (**A**) Monochromatic 70 keV image and (**B**) color-coded iodine map obtained using a single-source DECT system with fast kV switching, in a 51-year-old patient with bilateral renal masses. Note that the hypoattenuating lesion in the right kidney upper pole (*white arrow*) is displayed as devoid of iodine signal on the color-coded iodine map, indicating a nonenhancing hemorrhagic cyst; by comparison, the lesion in the left kidney lower pole (*white circle*) demonstrates an iodine signal on the color-coded map, reflecting its solid enhancing nature.

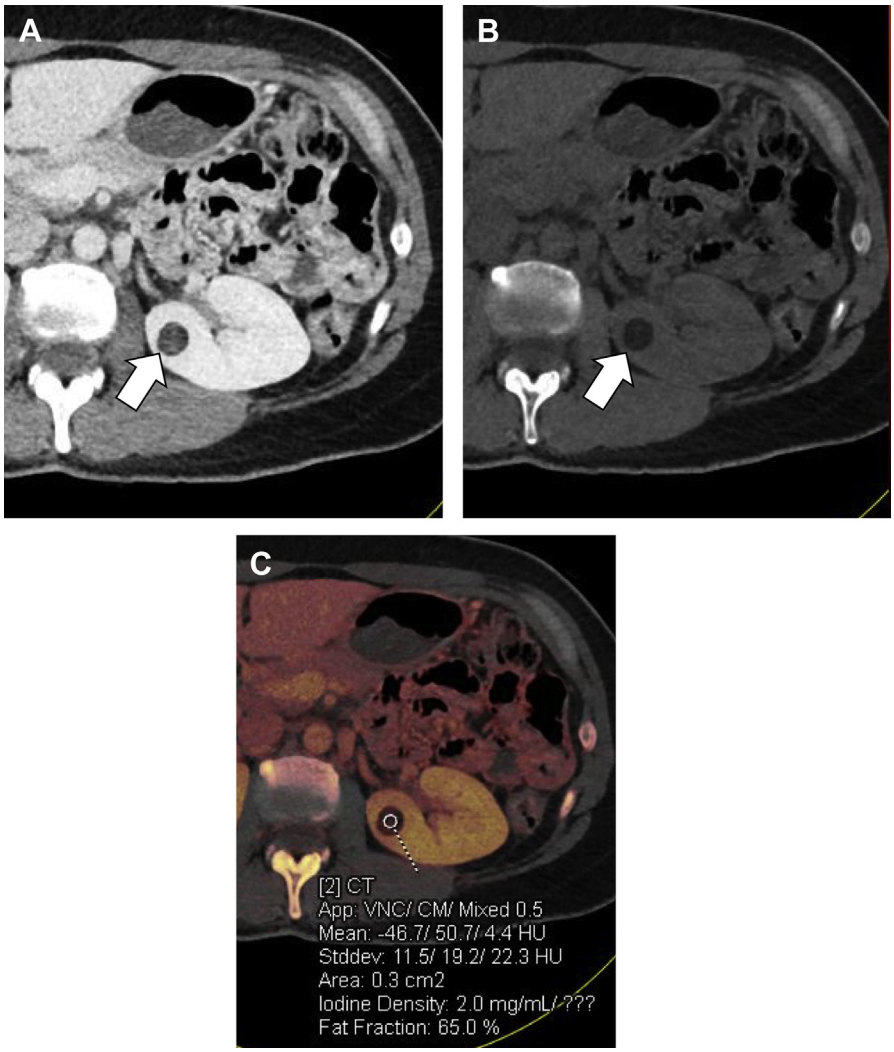

FIG. 4 (**A**) Mixed image, (**B**) virtual nonenhanced, and (**C**) color-coded map in a 36-year-old woman with angiomyolipoma of the left kidney (*white arrow*). Note that the region of interest drawn on the color-coded iodine map shows the fat fraction of the lesion.

enhancing nodules and masses have significantly higher contrast-to-noise ratio and visual conspicuity using 40 and 50 keV VMI reconstructions compared with routine polychromatic 120 kV images, but may demonstrate a slight increase in noise or artifacts [39–41]. Nevertheless, the overall benefit of the improved contrast-to-noise ratio translates into improved subjective conspicuity of arterially enhancing nodules for radiologists. Similar findings apply to iodine map images [42]. Iodine maps also improve the visualization of the ablation margin and residual neoplasms after chemoembolization, and iodine quantification can be used to detect portal vein tumor thrombus in equivocal cases [43,44]. On delayed images, Matsuda and colleagues [45] have shown that 50-keV images increase the conspicuity of tumor washout for small HCCs (Fig. 5).

At our institution, we perform contrast-enhanced, multiphase scanning for HCC using dual energy in the arterial and delayed phases (imaging only the abdomen), and single energy (with low tube potential technique) in the portal phase. Single tube energy portal phase images are used to identify the complications of portal hypertension (varices and shunts) with DECT 50 keV VMI and iodine maps supplementing mixed kV images in the arterial and delayed phase. Virtual

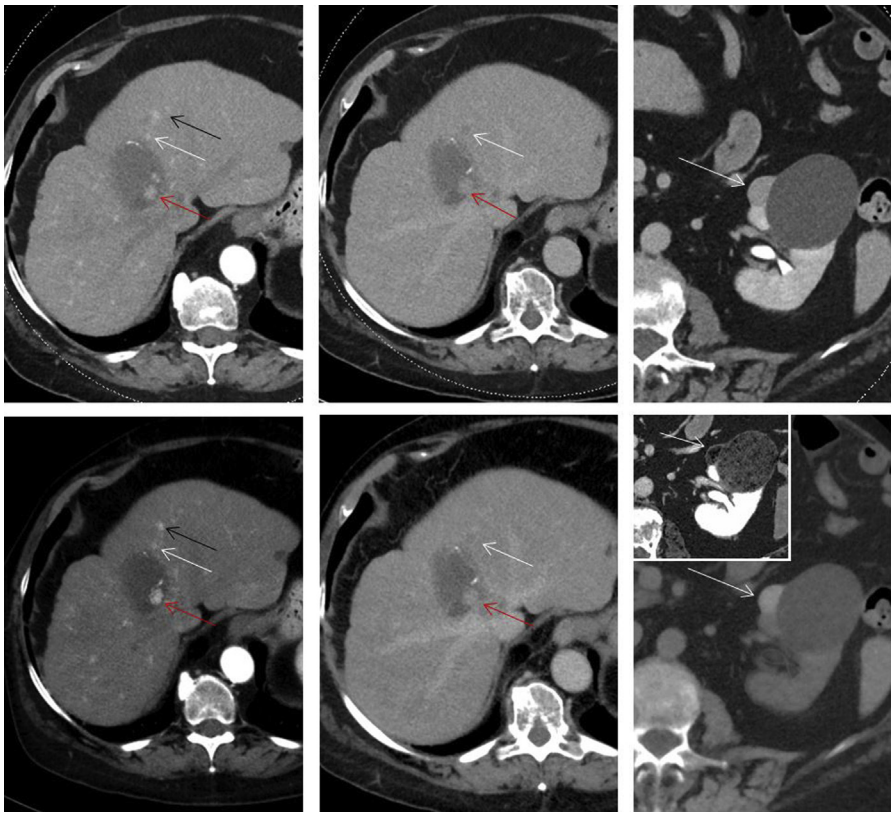

FIG. 5 Contrast-enhanced DECT performed to rule out residual HCC after chemoembolization demonstrated a large embolized HCC with an arterially enhancing residual tumor nodule, which is better seen on virtual monoenergetic 50 keV image (*red arrow*, *bottom left*) than mixed kV image (*red arrow*, *top left*). Delayed images also show tumor washout is better appreciated on the 50 keV image (*red arrow*, *bottom middle*). A small daughter lesion with arterial enhancement and washout is also seen at 50 keV (*white arrows*, *bottom left and middle*) compared with mixed kV images (*white arrows*, *top left and middle*), along with an indeterminate arterially enhancing nodule without washout (*black arrows*, *top left and bottom left*). In the same patient, a mixed kV image shows an indeterminate renal lesion (*white arrow*, *top right*), shown to be a hyperdense hemorrhage cyst on virtual noncontrast image (*white arrow*, *bottom right*). Iodine map image (*inset, bottom right*) shows no enhancement within the hemorrhagic cyst (*white arrow*, *inset bottom right*).

noncontrast images are reconstructed for the delayed phase only, because these images will be of higher quality than VNC images created from the arterial phase, owing to the improved discrimination of iodine at less than peak CT number.

Incorporating additional dual-energy images into multiphase liver CT image interpretation can maximize the benefit of dual-energy technology without excessively prolonging interpretation times if radiologists are willing to adopt a strategic approach to CT image interpretation. For example, 50 keV and iodine map images are evaluated only to detect arterially enhancing masses and tumor washout, and virtual noncontrast and iodine maps can be used to characterize incidental findings such as adrenal adenomas and indeterminate renal masses (see Fig. 5; Fig. 6).

Pancreaticobiliary Applications

DECT scanning can improve pancreatic CT imaging by potentiating iodine signal (similar to HCC) and discriminating between hemorrhage or iodine (similar to renal mass imaging). Additionally, a split bolus technique using single phase DECT scan with images reconstructed at 60 keV has been shown to demonstrate higher tumor conspicuity than conventional biphasic pancreatic CT examination at 120 kV [46].

Macari and colleagues [47] at New York University first introduced the concept that low kV or DECT scanning improves the identification of solid pancreatic masses. Investigators from the University of Alabama [48] have performed extensive investigations into the use of DECT scans for pancreatic cancer staging, and demonstrated that VMI at 52 keV demonstrate the largest CT number differences between tumors and adjacent pancreatic parenchyma, and that iodine maps increase reader confidence and tumor conspicuity. VMI reconstructions between 52 and 60 keV likely provide a useful trade-off to maximize tumor conspicuity and minimize noise and artifacts [49]. DECT scans at higher VMI energies can be used to decrease stent-related artifacts. For multiphase examinations, many use DECT scanning only for late arterial or pancreatic

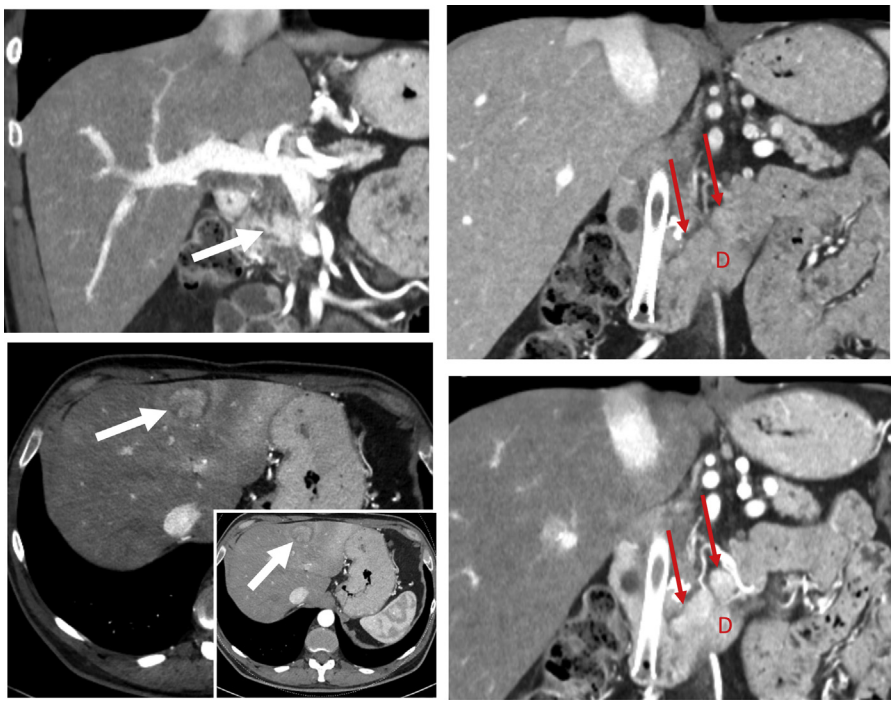

FIG. 6 Coronal 50 keV dual energy contrast-enhanced CT scan in the pancreatic phase shows a duct-obstructing hypervascular mass in the pancreatic neck (*white arrow*, *top left*). VMI better show hypervascular liver mass (shown to be an organizing abscess at biopsy) on 50 keV image (*white arrow*, *bottom left*) compared with mixed kV image (*white arrow*, *bottom left inset*). Coronal 50 keV image shows hypervascular nodal metastases (*red arrows, bottom right*) initially missed on review of mixed kV images (*top right*) located just superior to transverse duodenum (D, *right images*). Pathology revealed acinar cell carcinoma.

phases, where anticipated benefit is maximal [8]. DECT scanning is unlikely to be beneficial for improved characterization of cystic neoplasms, which are generally followed with MRI.

DECT scanning has diagnostic advantages in acute pancreatitis, where intraparenchymal hemorrhage and early necrosis are difficult to distinguish from poorly enhancing parenchyma. Imaging methods that can discriminate between hemorrhage or diminished perfusion improve identification of pancreatic necrosis [50]. Reconstruction of low-energy VMI and iodine maps can better display areas of enhancement and nonenhancement, and VNC images can be used to identify hemorrhage [51].

DECT scanning has been shown to increase absolute contrast difference between the noncalcified gallstones and surrounding bile most notable at 40 keV [52], permitting identification of a potential cause of abdominal pain and obviate the need for further imaging (Fig. 7).

Bowel Imaging Applications

Bowel masses and mucosal inflammation can be subtle on single energy CT scans, and gastrointestinal (GI) bleeding can mimic ingested hyperdense bowel contents. A DECT scan can be used to address these diagnostic challenges.

Acute gastrointestinal bleeding

The clinical manifestations of acute GI bleeding and their management and treatment depend on their source, the amount of the bleeding, and the general condition of the patient. Usually patients undergo upper or lower GI endoscopy as first line of management, which may localize or treat the bleeding source. For GI bleeding where endoscopic examination is inadequate, CT scanning has become an excellent alternative diagnostic tool because it can depict bleeding at a rate of 0.3 to 0.5 mL/min [53]. The role of CT is to identify the presence and location of active bleeding to plan for subsequent therapeutic (endoscopic, interventional, or surgical) approaches.

At our institute, we routinely use a DECT GI bleed protocol for the assessment of a patient presenting with an acute GI bleed. The study consists of bolus-tracked DECT arterial and DECT portal venous phase acquisition. If the patient is stable and small bowel pathology is suspected, the study can be performed as DECT enterography after giving neutral enteric contrast.

In metaanalysis, CT scanning showed high sensitivity (85%) and high specificity (92%) for detecting GI bleeding [54], and consists of a multiphase examination, often using unenhanced arterial and venous phase images. The most specific finding of active GI bleeding is the detection of active extravasation of iodine contrast into the bowel lumen on the arterial phase, with further pooling of contrast on the portal venous phase. Low keV images and iodine maps can, therefore, be used to increase the conspicuity of these findings (Fig. 8). If the intraluminal hyperattenuation observed on the iodine map disappears in the virtual nonenhanced images, it can be determined as intraluminal iodine content and is consistent with active extravasation (Fig. 9). The diagnostic accuracy in patients with active arterial bleeding of the abdomen can be significantly improved using noise optimized VMI reconstructions at 40 keV compared with standard linearly blended and traditional VMI series in DECT angiography [55].

Additionally, VNC images can replace conventional unenhanced images to characterize intraluminal hyperdense material (eg, hyperdense ingested food, surgical suture materials, residual barium in bowel that might be misconceived as active bleeding; Fig. 10) and result in a radiation dose reduction of approximately 30% when noncontrast acquisition is eliminated [56].

Luminal neoplasia

Colon cancer is often diagnosed with optical colonoscopy or CT colonography. Both of these procedures can require bowel preparation, colonic insufflation, sedation, and position changes, which can be difficult in the elderly population. Pilot studies suggest that DECT images may improve the detection of colorectal neoplasia without bowel preparation or improve electronic cleansing [57,58]. Density or visual analysis of iodine map and VNC DECT images allow accurate differentiation of tumor from stool by improving understanding of CT number heterogeneity, which is associated with stool [59].

Quantitative measurement of iodine content may aid in differentiating benign and aggressive colonic tumors [60]. The iodine density reflects tumor neovascularity and differentiation grades in gastric (Fig. 11) and colonic malignancies and is higher in poorly differentiated cancers than in moderately well-differentiated tumors [61,62]. The quantitative iodine density measurements can serve as markers of treatment response in malignancy and have been shown to be better markers than changes in tumor size [63].

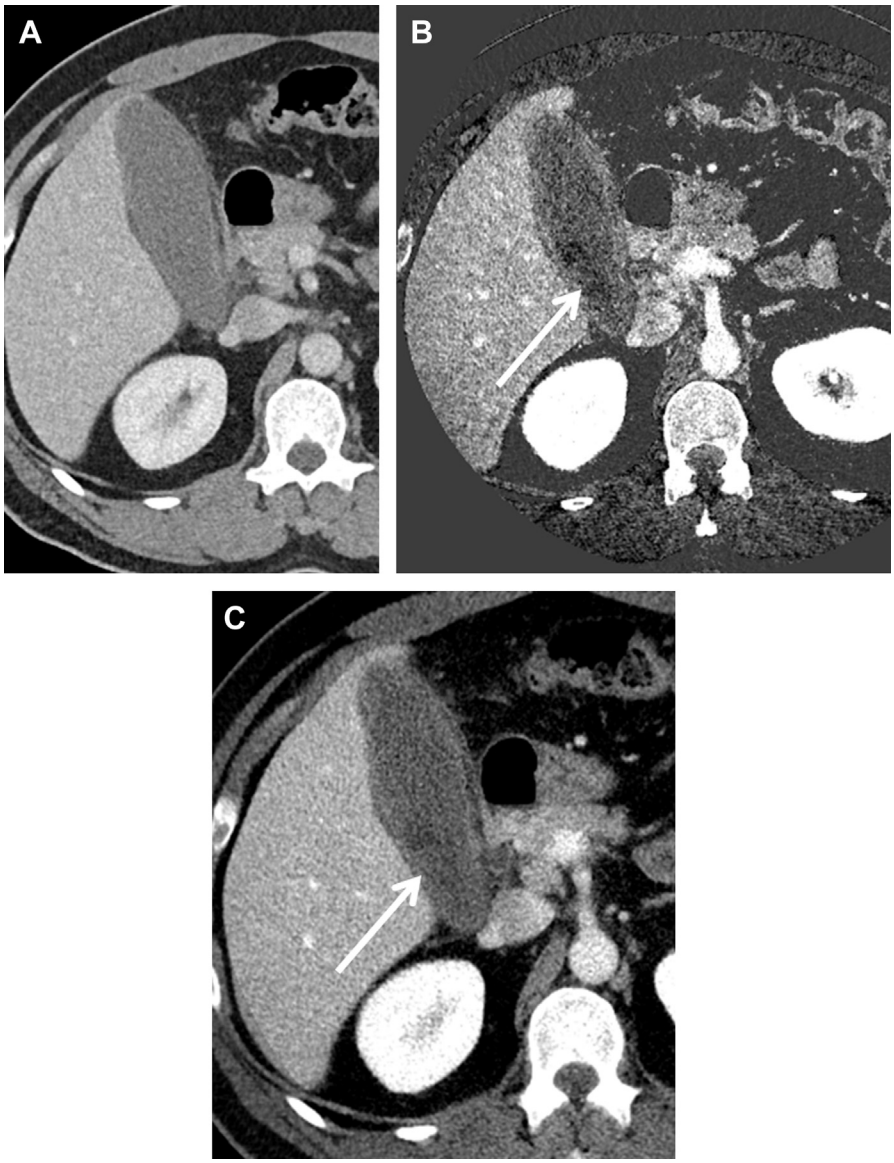

FIG. 7 Acute cholecystitis with a thickened gall bladder wall, but no gallstones visible on (**A**) mixed kV images. Noncalcified gallstones are seen only on (**B**) iodine map (*white arrow*) and (**C**) virtual monoenergetic 50 keV images (*white arrow*).

Infectious and inflammatory bowel disease

Nonspecific bowel thickening and surrounding fat stranding can suggest underlying enteritis or colitis in the appropriate clinical setting and is often encountered in patients presenting to the emergency room with abdominal pain, vomiting, or diarrhea.

DECT VMI and iodine maps may improve the conspicuity of inflammation and other abnormalities, particularly by accentuating alterations in bowel wall enhancement patterns through the use of iodine maps (Fig. 12) [64,65]. Recently, Elbanna and colleagues [66] demonstrated improved diagnostic accuracy with DECT for distinguishing gangrenous and

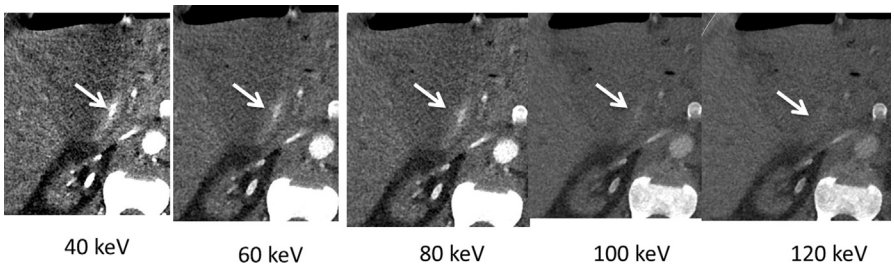

FIG. 8 Hyperdense duodenal bleed. Multiple axial VMI reconstructions at increasing energies (40–120 keV) show much greater signal associated with intraluminal extravasation of contrast (*arrows*) as VMI energy decreases. Low keV images are used to increase the conspicuity of subtle low-flow, low-volume bleeds.

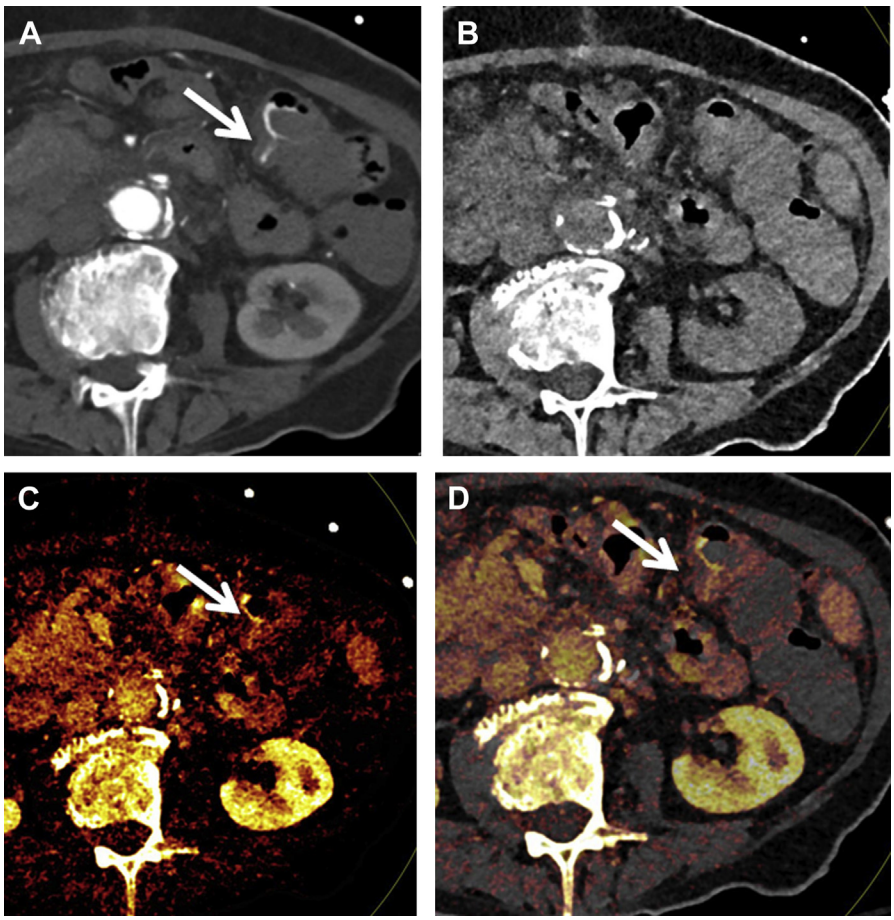

FIG. 9 A 74-year-old woman with bleeding per rectum. (**A**) Axial mixed CT image combines low- and high-kilovolt peak data to simulate a typical single-energy image and shows active arterial intraluminal extravasation of contrast (arrow in A,C and D) into the distal transverse colon in keeping with bleeding into diverticulum. (**B**) Axial virtual nonenhanced CT image was created by subtraction of the calculated iodine content, and does not show intraluminal iodine. (**C**) Axial iodine map image displays the intraluminal iodine content in color (arrow). (**D**) Axial iodine overlay image superimposes the color iodine map on the gray-scale virtual nonenhanced image.

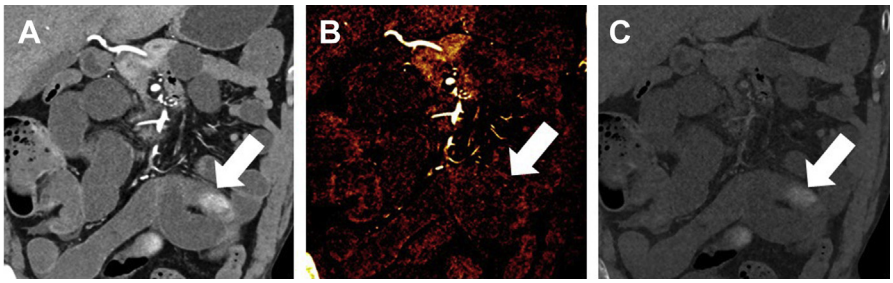

FIG. 10 Ingested material in a patient with suspected GI bleeding. (**A**) Coronal contrast-enhanced arterial phase CT image shows hyperattenuating material (*arrow*) in a small bowel loop in the left mid abdomen. The material disappears on the (**B**) coronal iodine map, but persists on (**C**) coronal virtual nonenhanced CT image, confirming that the finding does not represent active extravasation of iodine. The material was found to represent ingested bismuth.

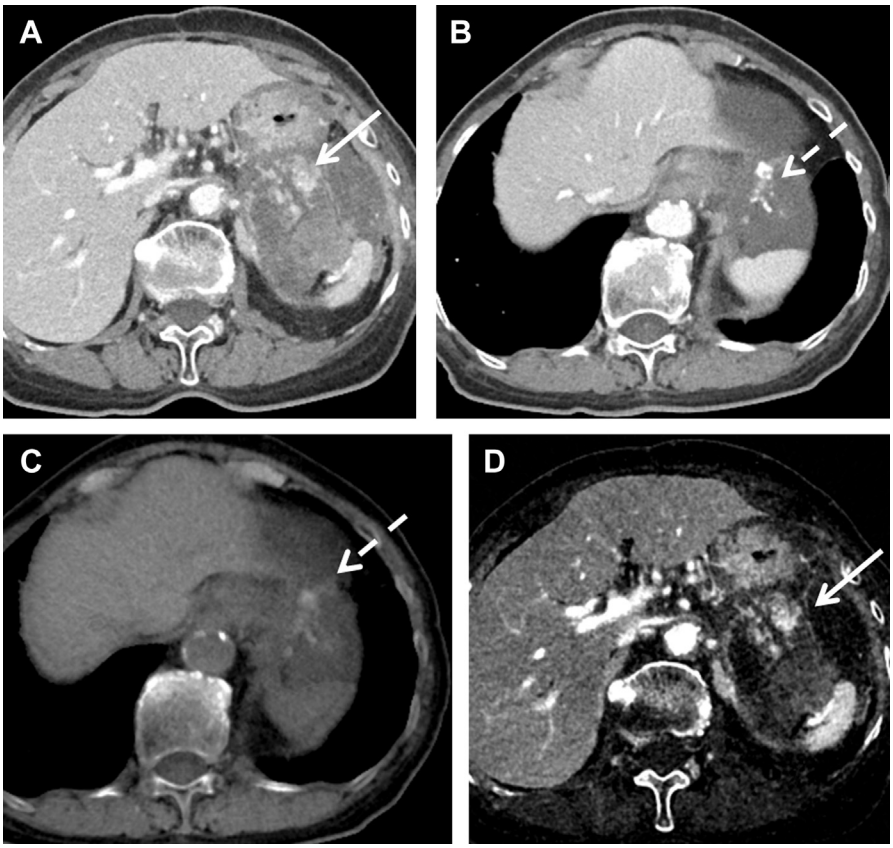

FIG. 11 (**A**, **B**) Axial mixed images show enhancing exophytic mass arising from the stomach, which was confirmed to be GI stromal tumor. The mass showed high density regions of enhancement (*continuous white arrow*) and calcifications (*dashed white arrow*), which are well-separated on (**C**) VNC and (**D**) iodine map images. Follow-up CT (not shown) shows decreased enhancement after therapy without much change in the size of the mass. These images demonstrate the ability of DECT scans to monitor treatment response.

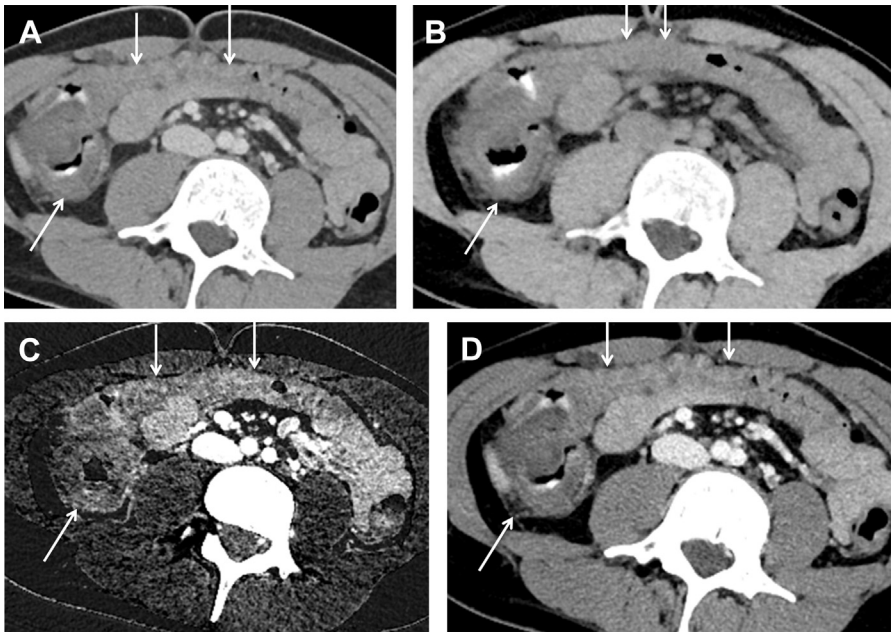

FIG. 12 A 65-year-old man presented with hematochezia and abdominal pain. (**A**) Axial mixed image shows marked colonic thickening (*white arrows*), which is asymmetrically greater in the cecum with increased surrounding fat stranding. High-density material the cecum was noted on (**B**) VNC images and not seen on iodine map images (**C**), confirming it to be ingested material rather than a bleed. Colonic wall hyperemia suggestive of acute colitis was accentuated on (**C**) iodine map and (**D**) virtual mono 50 keV images.

uncomplicated appendicitis owing to improved assessment of appendix wall on low keV images, which in turn can have significant management implications.

Ischemic bowel disease

Intestinal ischemia is surgical emergency requiring prompt diagnosis. It can be caused by thromboembolic disease, low-flow state hypoperfusion, or secondary causes such as bowel obstruction [67]. Bowel wall hypoenhancement is the most specific sign of ischemia at CT scanning (93%–100%), but has a high likelihood of going unrecognized [68]. The iodine density map and the VMI at low keV increase the conspicuity of acute bowel ischemia, resulting in improved diagnostic accuracy compared with the conventional image alone [69]. The relative enhancement of the abnormal bowel can be compared with adjacent loops. DECT VNC images can also aid in the identification of bowel hemorrhage, another manifestation of bowel ischemia (Fig. 13).

Trauma

The advent of DECT scanning has reinforced the use of CT scans in the acute setting, with their potentially added clinical benefit. Trauma is the leading cause of death in young patients. Both iodine-selective imaging and virtual monoenergetic imaging can increase the conspicuity of traumatic solid organ and hollow visceral injuries, making injuries easier to detect and categorize. Iodine-selective imaging, through the use of iodine maps and virtual noncontrast images, can assist in the evaluation of active contrast extravasation by differentiating it from other hyperdense lesions, such as foreign body or osseous fragments from fractures [70]. Similar to VNC images that subtract iodine, DECT postprocessing can also subtract trabecular bone to create virtual noncalcium images, which can unmask bone marrow edema, improving the detection of subtle fractures. High keV monoenergetic images can decrease metal artifact, which may be helpful in assessing for traumatic injury in cases of penetrating trauma [71].

STANDARDIZATION OF DISPLAYS

Virtual monoenergetic displays should be routinely generated when using dual energy images in the abdomen and pelvis. Most institutions use 50 to

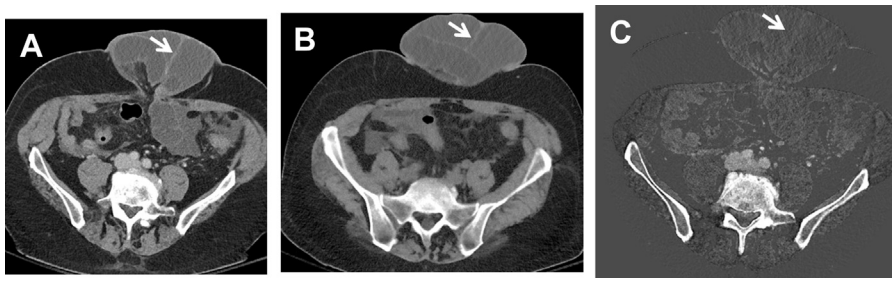

FIG. 13 A 56-year-old man with acute abdominal pain and vomiting. (**A**) DECT axial mixed images showing an obstructed umbilical hernia with a hyperattenuating wall (*arrow*). This was confirmed to be bowel wall hemorrhage on (**B**) VNC images, and (**C**) iodine-only images showed no enhancement in the wall suggestive of bowel ischemia.

60 keV images to potentiate iodine signal and higher keV images (eg, 100 keV) to decrease beam hardening owing to metal artifacts (when present). Although conventional CT numbers (ie, Hounsfield units) are routinely used in abdominal imaging for many clinical scenarios, it should be recognized that CT numbers from traditional CT scans vary according to patient attenuation, because beam hardening changes the CT number observed on single energy CT scans. VMI have Hounsfield unit numbers that are different from those obtained at 120 kV, but they are consistent across patient sizes [72]. The stability of CT numbers across patients should improve diagnostic recommendation based on CT number and offer opportunities for using CT numbers more reliably in surveillance imaging (eg, to gauge tumor response).

Virtual Noncontrast Imaging Strengths and Weaknesses

Some benefits and limitations of VNC images have already been reviewed, but radiologists should also consider the contrast-enhanced series from which VNC images are created [73,74]. VNC images based on arterial phase CT angiography have significantly higher mean attenuation and noise levels compared with traditional noncontrast images and may result in incomplete iodine removal [75]; consequently, VNC images should be created from later phases of enhancement [76]. Future optimizations of material decomposition algorithms are likely to overcome present discrepancy in true and VNC attenuation measurement differences.

Matched Use of Virtual Noncontrast Imaging and Iodine Maps

Iodine overlay images that superimpose the iodine content in color on top of the gray-scale virtual nonenhanced image can be obtained to visualize the iodine content of a tissue or a lesion. Iodine concentration in milligrams per milliliter can be obtained from these images. Iodine images can be shown by themselves or as an overlay on top of a conventional CT image. One must view both iodine and water/VNC images as a pair to best distinguish between low levels of enhancement and hemorrhage.

LOW IODINE IMAGING

In high-risk patients with renal dysfunction, the American College of Radiology recommends more restricted contrast use. Low keV images accentuate iodine content within structures, thus opening up possibilities to decrease the contrast dose while maintaining the image quality and diagnostic performance. At our institution we have developed DE-based, low iodine CT protocols that can often decrease the contrast volume and iodine dose to less than 50%, depending on the body mass index of patient. This modality is especially useful in situations where minimizing contrast dose is desired without compromising the added benefit of contrast enhanced study compared with unenhanced CT scans [77].

WORKFLOW AND INTEGRATION INTO HETEROGENEOUS PRACTICES

There continues to be significant variation in practice patterns and applications of the technology. To make use of DECT in routine clinical practice, most image processing must be performed in the background by the scanner. Our optimized workflow includes automatically generated, mixed kV images that accentuate iodine signal (0.6 linear blend), VNC images, 50 keV VMI and iodine map images by the scanner and sent to PACS, along with routine coronal and sagittal reformatted

images. Incorporation of a fully automated DECT postprocessing workflow eliminates additional steps from the technologists, resulting in a marked increase in the proportion of scans containing the desired DECT image series, and a large reduction in processing delays. In our department, we emphasize indication-based CT protocols specific to DECT scanning to minimize the number of additional series. This practice helps radiologists to recognize that postprocessed images are often used for problem solving after evaluating mixed kV images, thus minimally impacting interpretation time.

PHOTON-COUNTING COMPUTED TOMOGRAPHY

In addition to the current commercial implementations, photon counting detector (PCD) CT scanning is an emerging option to achieve DECT or multienergy CT scans. Although it is currently not available commercially, early results from research systems have demonstrated great potential of PCD-CT scanning in various clinical areas.

Conventional CT detectors use a scintillator layer to convert detected x-ray photons into visible light, which is consequently converted into electronic signals through photo diodes. In PCD CT, x-ray photons are directly converted into electronic signals without generating the intermediate visible light like the traditional energy integrating CT detectors. The final detector signal is proportional to the number of detected photons, with signals from different photons grouped according to multiple (usually 2 – 8) energy bins. Owing to its capability of counting individual photon and discriminating its energy, PCD-CT has benefits over energy integrating detectors in terms of reduced electronic noise, increased contrast and contrast-to-noise ratio, reduced beam hardening and metal artifacts, and simultaneous high-resolution and multienergy imaging [78].

Given its energy discrimination capability, PCD-CT scanning achieves simultaneous multienergy CT scanning without any misregistration using a single tube and single tube energy [79]. Material specific images, such as iodine map and virtual noncontrast images, have been created using PCD-CT. Initial results have demonstrated accurate iodine quantification and accurate CT number of VMI using PCD-CT [80] as well as improved ability to characterize small renal stones [23].

SUMMARY

Using advanced dual-energy imaging, a more precise diagnosis can often be obtained with a greater degree of confidence. Dual energy CT holds promising potential for use as an imaging biomarker, for risk stratification, for the monitoring of disease progression and therapy, and for outcome prediction.

REFERENCES

[1] Fletcher JG, Takahashi N, Hartman R, et al. Dual-energy and dual-source CT: is there a role in the abdomen and pelvis? Radiol Clin North Am 2009;47(1):41–57.
[2] Flohr TG, McCollough CH, Bruder H, et al. First performance evaluation of a dual-source CT (DSCT) system. Eur Radiol 2006;16(2):256–68.
[3] Rassouli N, Etesami M, Dhanantwari A, et al. Detector-based spectral CT with a novel dual-layer technology: principles and applications. Insights Imaging 2017;8(6):589–98.
[4] Zhang D, Li X, Liu B. Objective characterization of GE discovery CT750 HD scanner: gemstone spectral imaging mode. Med Phys 2011;38(3):1178–88.
[5] Siegel MJ, Kaza RK, Bolus DN, et al. White paper of the Society of Computed Body Tomography and Magnetic Resonance on Dual-Energy CT, part 1: technology and terminology. J Comput Assist Tomogr 2016;40(6):841–5.
[6] De Cecco CN, Boll DT, Bolus DN, et al. White paper of the Society of Computed Body Tomography and Magnetic Resonance on Dual-Energy CT, part 4: abdominal and pelvic applications. J Comput Assist Tomogr 2017;41(1):8–14.
[7] McCollough CH, Leng S, Yu L, et al. Dual- and multi-energy CT: principles, technical approaches, and clinical applications. Radiology 2015;276(3):637–53.
[8] Patel BN, Alexander L, Allen B, et al. Dual-energy CT workflow: multi-institutional consensus on standardization of abdominopelvic MDCT protocols. Abdom Radiol (NY) 2017;42(3):676–87.
[9] Leng S, Yu L, Fletcher JG, et al. maximizing iodine contrast-to-noise ratios in abdominal CT imaging through use of energy domain noise reduction and virtual monoenergetic dual-energy CT. Radiology 2015;276(2):562–70.
[10] Leng S, Yu L, Wang J, et al. Noise reduction in spectral CT: reducing dose and breaking the trade-off between image noise and energy bin selection. Med Phys 2011;38(9):4946–57.
[11] Caoili EM, Korobkin M, Francis IR, et al. Adrenal masses: characterization with combined unenhanced and delayed enhanced CT. Radiology 2002;222(3):629–33.
[12] Song JH, Mayo-Smith WW. Incidentally discovered adrenal mass. Radiol Clin North Am 2011;49(2):361–8.
[13] Gupta RT, Ho LM, Marin D, et al. Dual-energy CT for characterization of adrenal nodules: initial experience. AJR Am J Roentgenol 2010;194(6):1479–83.
[14] Ho LM, Marin D, Neville AM, et al. Characterization of adrenal nodules with dual-energy CT: can virtual

unenhanced attenuation values replace true unenhanced attenuation values? AJR Am J Roentgenol 2012;198(4):840–5.
[15] Martin SS, Weidinger S, Czwikla R, et al. Iodine and fat quantification for differentiation of adrenal gland adenomas from metastases using third-generation dual-source dual-energy computed tomography. Invest Radiol 2018;53(3):173–8.
[16] Morgan DE, Weber AC, Lockhart ME, et al. Differentiation of high lipid content from low lipid content adrenal lesions using single-source rapid kilovolt (peak)-switching dual-energy multidetector CT. J Comput Assist Tomogr 2013;37(6):937–43.
[17] Mileto A, Nelson RC, Marin D, et al. Dual-energy multidetector CT for the characterization of incidental adrenal nodules: diagnostic performance of contrast-enhanced material density analysis. Radiology 2015;274(2):445–54.
[18] Glazer DI, Maturen KE, Kaza RK, et al. Adrenal Incidentaloma triage with single-source (fast-kilovoltage switch) dual-energy CT. AJR Am J Roentgenol 2014;203(2):329–35.
[19] Primak AN, Fletcher JG, Vrtiska TJ, et al. Noninvasive differentiation of uric acid versus non-uric acid kidney stones using dual-energy CT. Acad Radiol 2007;14(12):1441–7.
[20] Graser A, Johnson TR, Bader M, et al. Dual energy CT characterization of urinary calculi: initial in vitro and clinical experience. Invest Radiol 2008;43(2):112–9.
[21] Leng S, Shiung M, Ai S, et al. Feasibility of discriminating uric acid from non-uric acid renal stones using consecutive spatially registered low- and high-energy scans obtained on a conventional CT scanner. AJR Am J Roentgenol 2015;204(1):92–7.
[22] Duan X, Li Z, Yu L, et al. Characterization of urinary stone composition by use of third-generation dual-source dual-energy CT with increased spectral separation. AJR Am J Roentgenol 2015;205(6):1203–7.
[23] Marcus RP, Fletcher JG, Ferrero A, et al. Detection and characterization of renal stones by using photon-counting-based CT. Radiology 2018;289(2):436–42.
[24] Suh M, Coakley FV, Qayyum A, et al. Distinction of renal cell carcinomas from high-attenuation renal cysts at portal venous phase contrast-enhanced CT. Radiology 2003;228(2):330–4.
[25] Birnbaum BA, Hindman N, Lee J, et al. Multi-detector row CT attenuation measurements: assessment of intra- and interscanner variability with an anthropomorphic body CT phantom. Radiology 2007;242(1):109–19.
[26] Mileto A, Nelson RC, Paulson EK, et al. Dual-energy MDCT for imaging the renal mass. AJR Am J Roentgenol 2015;204(6):W640–7.
[27] Ascenti G, Mazziotti S, Mileto A, et al. Dual-source dual-energy CT evaluation of complex cystic renal masses. AJR Am J Roentgenol 2012;199(5):1026–34.
[28] Graser A, Johnson TR, Hecht EM, et al. Dual-energy CT in patients suspected of having renal masses: can virtual nonenhanced images replace true nonenhanced images? Radiology 2009;252(2):433–40.
[29] Song KD, Kim CK, Park BK, et al. Utility of iodine overlay technique and virtual unenhanced images for the characterization of renal masses by dual-energy CT. AJR Am J Roentgenol 2011;197(6):W1076–82.
[30] Marin D, Davis D, Roy Choudhury K, et al. Characterization of small focal renal lesions: diagnostic accuracy with single-phase contrast-enhanced dual-energy CT with material attenuation analysis compared with conventional attenuation measurements. Radiology 2017;284(3):737–47.
[31] Chandarana H, Megibow AJ, Cohen BA, et al. Iodine quantification with dual-energy CT: phantom study and preliminary experience with renal masses. AJR Am J Roentgenol 2011;196(6):W693–700.
[32] Kaza RK, Platt JF, Cohan RH, et al. Dual-energy CT with single- and dual-source scanners: current applications in evaluating the genitourinary tract. Radiographics 2012;32(2):353–69.
[33] Mileto A, Marin D, Ramirez-Giraldo JC, et al. Accuracy of contrast-enhanced dual-energy MDCT for the assessment of iodine uptake in renal lesions. AJR Am J Roentgenol 2014;202(5):W466–74.
[34] Mileto A, Barina A, Marin D, et al. Virtual monochromatic images from dual-energy multidetector CT: variance in CT numbers from the same lesion between single-source projection-based and dual-source image-based implementations. Radiology 2016;279(1):269–77.
[35] Mileto A, Allen BC, Pietryga JA, et al. Characterization of incidental renal mass with dual-energy CT: diagnostic accuracy of effective atomic number maps for discriminating nonenhancing cysts from enhancing masses. AJR Am J Roentgenol 2017;209(4):W221–30.
[36] Mileto A, Marin D. Dual-energy computed tomography in genitourinary imaging. Radiol Clin North Am 2017;55(2):373–91.
[37] Arslanoglu A, Seyal AR, Sodagari F, et al. Current guidelines for the diagnosis and management of hepatocellular carcinoma: a comparative review. AJR Am J Roentgenol 2016;207(5):W88–98.
[38] Purysko AS, Primak AN, Baker ME, et al. Comparison of radiation dose and image quality from single-energy and dual-energy CT examinations in the same patients screened for hepatocellular carcinoma. Clin Radiol 2014;69(12):e538–44.
[39] Husarik DB, Gordic S, Desbiolles L, et al. Advanced virtual monoenergetic computed tomography of hyperattenuating and hypoattenuating liver lesions: ex-vivo and patient experience in various body sizes. Invest Radiol 2015;50(10):695–702.
[40] Shuman WP, Green DE, Busey JM, et al. Model-based iterative reconstruction versus adaptive statistical iterative reconstruction and filtered back projection in liver 64-MDCT: focal lesion detection, lesion conspicuity, and image noise. AJR Am J Roentgenol 2013;200(5):1071–6.

[41] Hanson GJ, Michalak GJ, Childs R, et al. Low kV versus dual-energy virtual monoenergetic CT imaging for proven liver lesions: what are the advantages and trade-offs in conspicuity and image quality? A pilot study. Abdom Radiol (NY) 2018;43(6):1404–12.
[42] Pfeiffer D, Parakh A, Patino M, et al. Iodine material density images in dual-energy CT: quantification of contrast uptake and washout in HCC. Abdom Radiol (NY) 2018; 43(12):3317–23.
[43] Ascenti G, Sofia C, Mazziotti S, et al. Dual-energy CT with iodine quantification in distinguishing between bland and neoplastic portal vein thrombosis in patients with hepatocellular carcinoma. Clin Radiol 2016;71(9): 938.e1-9.
[44] Lee SH, Lee JM, Kim KW, et al. Dual-energy computed tomography to assess tumor response to hepatic radiofrequency ablation: potential diagnostic value of virtual noncontrast images and iodine maps. Invest Radiol 2011;46(2):77–84.
[45] Matsuda M, Tsuda T, Kido T, et al. Dual-energy computed tomography in patients with small hepatocellular carcinoma: utility of noise-reduced monoenergetic images for the evaluation of washout and image quality in the equilibrium phase. J Comput Assist Tomogr 2018; 42(6):937–43.
[46] Brook OR, Gourtsoyianni S, Brook A, et al. Split-bolus spectral multidetector CT of the pancreas: assessment of radiation dose and tumor conspicuity. Radiology 2013;269(1):139–48.
[47] Macari M, Spieler B, Kim D, et al. Dual-source dual-energy MDCT of pancreatic adenocarcinoma: initial observations with data generated at 80 kVp and at simulated weighted-average 120 kVp. AJR Am J Roentgenol 2010;194(1):W27–32.
[48] McNamara MM, Little MD, Alexander LF, et al. Multireader evaluation of lesion conspicuity in small pancreatic adenocarcinomas: complimentary value of iodine material density and low keV simulated monoenergetic images using multiphasic rapid kVp-switching dual energy CT. Abdom Imaging 2015; 40(5):1230–40.
[49] Frellesen C, Fessler F, Hardie AD, et al. Dual-energy CT of the pancreas: improved carcinoma-to-pancreas contrast with a noise-optimized monoenergetic reconstruction algorithm. Eur J Radiol 2015;84(11):2052–8.
[50] Tsuji Y, Takahashi N, Fletcher JG, et al. Subtraction color map of contrast-enhanced and unenhanced CT for the prediction of pancreatic necrosis in early stage of acute pancreatitis. AJR Am J Roentgenol 2014; 202(4):W349–56.
[51] Almeida RR, Lo GC, Patino M, et al. Advances in pancreatic CT imaging. AJR Am J Roentgenol 2018;211(1): 52–66.
[52] Uyeda JW, Richardson IJ, Sodickson AD. Making the invisible visible: improving conspicuity of noncalcified gallstones using dual-energy CT. Abdom Radiol (NY) 2017;42(12):2933–9.
[53] Wells ML, Hansel SL, Bruining DH, et al. CT for evaluation of acute gastrointestinal bleeding. Radiographics 2018;38(4):1089–107.
[54] Garcia-Blazquez V, Vicente-Bartulos A, Olavarria-Delgado A, et al. Accuracy of CT angiography in the diagnosis of acute gastrointestinal bleeding: systematic review and meta-analysis. Eur Radiol 2013;23(5): 1181–90.
[55] Martin SS, Wichmann JL, Scholtz JE, et al. Noise-optimized virtual monoenergetic dual-energy CT Improves diagnostic accuracy for the detection of active arterial bleeding of the abdomen. J Vasc Interv Radiol 2017; 28(9):1257–66.
[56] Sun H, Hou XY, Xue HD, et al. Dual-source dual-energy CT angiography with virtual non-enhanced images and iodine map for active gastrointestinal bleeding: image quality, radiation dose and diagnostic performance. Eur J Radiol 2015;84(5):884–91.
[57] Boellaard TN, Henneman OD, Streekstra GJ, et al. The feasibility of colorectal cancer detection using dual-energy computed tomography with iodine mapping. Clin Radiol 2013;68(8):799–806.
[58] Tachibana R, Nappi JJ, Ota J, et al. Deep learning electronic cleansing for single- and dual-energy CT colonography. Radiographics 2018;38(7):2034–50.
[59] Ozdeniz I, Idilman IS, Koklu S, et al. Dual-energy CT characteristics of colon and rectal cancer allows differentiation from stool by dual-source CT. Diagn Interv Radiol 2017;23(4):251–6.
[60] Schaeffer B, Johnson TR, Mang T, et al. Dual-energy CT colonography for preoperative "one-stop" staging in patients with colonic neoplasia. Acad Radiol 2014;21(12): 1567–72.
[61] Chuang-Bo Y, Tai-Ping H, Hai-Feng D, et al. Quantitative assessment of the degree of differentiation in colon cancer with dual-energy spectral CT. Abdom Radiol (NY) 2017;42(11):2591–6.
[62] Liang P, Ren XC, Gao JB, et al. Iodine concentration in spectral CT: assessment of prognostic determinants in patients with gastric adenocarcinoma. AJR Am J Roentgenol 2017;209(5):1033–8.
[63] Tang L, Li ZY, Li ZW, et al. Evaluating the response of gastric carcinomas to neoadjuvant chemotherapy using iodine concentration on spectral CT: a comparison with pathological regression. Clin Radiol 2015;70(11): 1198–204.
[64] Fulwadhva UP, Wortman JR, Sodickson AD. Use of dual-energy CT and iodine maps in evaluation of bowel disease. Radiographics 2016;36(2):393–406.
[65] Lee SM, Kim SH, Ahn SJ, et al. Virtual monoenergetic dual-layer, dual-energy CT enterography: optimization of keV settings and its added value for Crohn's disease. Eur Radiol 2018;28(6):2525–34.
[66] Elbanna KY, Mohammed MF, Chahal T, et al. Dual-energy CT in differentiating nonperforated gangrenous appendicitis from uncomplicated appendicitis. AJR Am J Roentgenol 2018;211(4):776–82.

[67] Olson MC, Fletcher JG, Nagpal P, et al. Mesenteric ischemia: what the radiologist needs to know. Cardiovasc Diagn Ther 2018.
[68] Potretzke TA, Brace CL, Lubner MG, et al. Early small-bowel ischemia: dual-energy CT improves conspicuity compared with conventional CT in a swine model. Radiology 2015;275(1):119–26.
[69] Lourenco PDM, Rawski R, Mohammed MF, et al. Dual-energy CT iodine mapping and 40-keV monoenergetic applications in the diagnosis of acute bowel ischemia. AJR Am J Roentgenol 2018;211(3):564–70.
[70] Wortman JR, Uyeda JW, Fulwadhva UP, et al. Dual-energy CT for abdominal and pelvic trauma. Radiographics 2018;38(2):586–602.
[71] Park J, Kim SH, Han JK. Combined application of virtual monoenergetic high keV images and the orthopedic metal artifact reduction algorithm (O-MAR): effect on image quality. Abdom Radiol (NY) 2019;44(2):756–65.
[72] Michalak G, Grimes J, Fletcher J, et al. Technical note: improved CT number stability across patient size using dual-energy CT virtual monoenergetic imaging. Med Phys 2016;43(1):513.
[73] De Cecco CN, Buffa V, Fedeli S, et al. Dual energy CT (DECT) of the liver: conventional versus virtual unenhanced images. Eur Radiol 2010;20(12):2870–5.
[74] Durieux P, Gevenois PA, Muylem AV, et al. Abdominal attenuation values on virtual and true unenhanced images obtained with third-generation dual-source dual-energy CT. AJR Am J Roentgenol 2018;210(5):1042–58.
[75] Lehti L, Soderberg M, Hoglund P, et al. Reliability of virtual non-contrast computed tomography angiography: comparing it with the real deal. Acta Radiol Open 2018;7(7–8):2058460118790115.
[76] Kaza RK, Raff EA, Davenport MS, et al. Variability of CT attenuation measurements in virtual unenhanced images generated using multimaterial decomposition from fast kilovoltage-switching dual-energy CT. Acad Radiol 2017;24(3):365–72.
[77] Deinzer CK, Danova D, Kleb B, et al. Influence of different iodinated contrast media on the induction of DNA double-strand breaks after in vitro X-ray irradiation. Contrast Media Mol Imaging 2014;9(4):259–67.
[78] Leng S, Bruesewitz MR, Tao S, et al. Photon counting detector CT: system design and clinical applications of an emerging technology. RadioGraphics 2019;29:729–43.
[79] Yu Z, Leng S, Jorgensen SM, et al. Evaluation of conventional imaging performance in a research whole-body CT system with a photon-counting detector array. Phys Med Biol 2016;61(4):1572–95.
[80] Leng S, Zhou W, Yu Z, et al. Spectral performance of a whole-body research photon counting detector CT: quantitative accuracy in derived image sets. Phys Med Biol 2017;62(17):7216–32.